Inorganic Chemistry

Article

pubs.acs.org/IC

Polynuclear Fe_n Complexes (n = 1, 2, 4, 5) of Polytopic Hydrazone Ligands with Fe(II), Fe(III) and Mixed Oxidation State Combinations

Muhammad U. Anwar, Konstantin V. Shuvaev, Louise N. Dawe, and Laurence K. Thompson*

Department of Chemistry, Memorial University, St. John's Newfoundland, A1B 3X7, Canada

Supporting Information

ABSTRACT: The iron coordination chemistry of some polytopic hydrazone based ligands is examined. The complexes derive from a general self-assembly strategy, where ligand design can be used to devise specific polymetallic [$n \times n$] grid architectures. However, as part of any complex equilibrium process, oligomeric entities can also occur, particularly when ligand tautomeric flexibility is considered, and examples of mononuclear, dinuclear, tetranuclear, and pentanuclear complexes have been observed within a related class of ligands. In addition, ligand site donor composition can lead to coordination spheres that stabilize both high spin Fe(II) and Fe(III) sites, with evidence for Fe(II) spin crossover. Structural and magnetic properties are examined, which reveal the presence of antiferromagnetic exchange in the polynuclear systems.

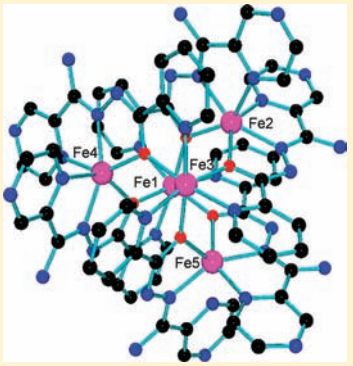

INTRODUCTION

The coordination chemistry of iron is complicated by its propensity to undergo redox reactions, often triggered by exposure to air, but also by the influence of the ligand field environment on its spin state situation. The literature abounds with papers on Fe(II), and to a lesser extent Fe(III) systems, in high spin (HS) and low spin (LS) states, and there is evidence for a variety of factors which contribute to this situation, including the ligand field environment. A comprehensive monograph on properties of such systems covers this broad research area.[1] Generally a fairly strong ligand field is required to cause a HS Fe(II) system to undergo spin crossover to the LS state within the normally accessible temperature limits (e.g., 2−300 K). The now classic Fe(II)-triazole polymeric chain compounds studied by Kahn and co-workers,[2−4] which undergo spin transition behavior and thermo-chromism,[4,5] provide a bistable molecule-based medium suitable for a display device, which came close to commercial utility.[3] The Fe(II) centers have N_6 coordination spheres.

Synthetic polynuclear iron clusters have been a focus of attention because of their novel bulk magnetic properties, perhaps as a result of the traditional use of iron oxide magnetic particles as magnetic media, and the presence of natural (biological) examples of magnetic iron oxide based clusters (e.g., ferritin).[6] Single molecule magnet behavior has been observed with both Fe(II) and Fe(III) examples.[7−9] These types of clusters result in large measure through serendipitous synthesis, starting with relatively simple coordinatively unsaturated ligands, which create clusters of varying dimensions through a divergent approach, where the limited numbers of donors on a primary ligand force the metals to form aggregate structures resulting from single atom, for example, oxygen and carboxylate bridges, which arise from both endogenous and exogenous sources. In our studies we have focused on what can be described as a convergent approach, where, through encoding of coordination information in the primary polydentate, polytopic ligand, directed assemblies of specific polynuclear architectures can be created. Polytopic hydrazones have provided a wealth of opportunities to generate square self-assembled [$n \times n$] grid structures (n = 2−5), where a key structural feature of the ligand is the contiguous linear arrangement of NO based tridentate coordination pockets, which lead to the formation of five-membered chelate rings. Typical ligands include poap and derivatives (ditopic), and 2poap and derivatives (tritopic) (Chart 1), which lead successfully to self-assembled square tetranuclear [2 × 2] and nonanuclear [3 × 3] grids respectively. M_4 [2 × 2] systems have been produced with Mn(II), Ni(II), Co(II), Cu(II), and Zn(II) salts,[10−12] while well documented examples of [3 × 3] systems have so far been limited to Mn(II), Cu(II), and Zn(II), and just one Co(II) example to date.[13−20]

Iron chemistry with pyridine-hydrazone ligands in this class has been much more limited, with structurally documented examples of mononuclear (HS Fe(III)),[21] dinuclear (LS Fe(II)[22] systems, and a pentanuclear (HS Fe(III))[17] system, based on a symmetrical incomplete [3 × 3] grid motif, with Fe(III) at the center and side sites of a typical square grid-like arrangement of six ligands. No examples of [2 × 2] or complete [3 × 3] iron grids have been reported so far with this type of

Received: August 29, 2011
Published: October 26, 2011

Chart 1

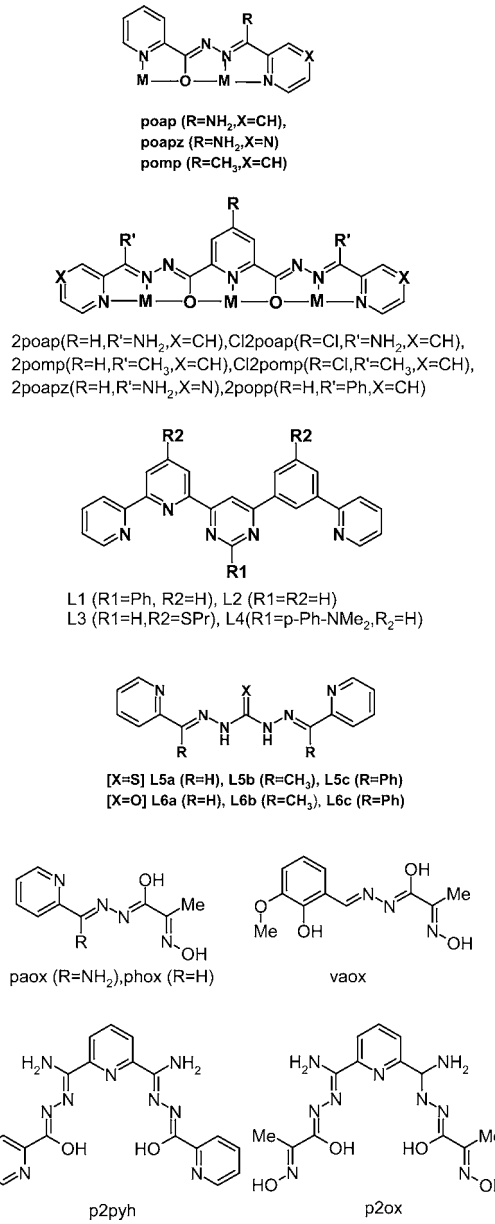

ligand. A few examples of [2 × 2] iron grids have been reported with ditopic ligands based on pyrimidine, and thiocarbohydrazide bridging fragments. The complex $[Fe(II)_4(L1)_4](ClO_4)_8$ (Chart 1) consists of four six-coordinate $Fe(II)N_6$ centers bridged by pyrimidine groups. Spin crossover is observed, promoted by temperature, pressure, and light.[23] Substituent effects (Chart 1; L1−L4; R1, R2) in this class of ligand lead to modulation of the crystal field and in response a differing tendency to stabilize the LS Fe(II) state. With L2, L3, and L4 only the LS state is observed, while for ligands in which R1 = Me, Ph temperature dependent spin transition behavior is observed.[24]

The facile redox behavior of iron (Fe(III)/Fe(II) reduction potential E^0 = 0.771 V), means that in the presence of air iron(II) oxidation can occur, and so the observation of oxidized or mixed oxidation state species might be anticipated. Mixed S/N ligands, for example, L5a-c, based on thiocarbohydrazone, create quite strong crystal fields.[25,26] Examples of mixed oxidation state Fe(II)/Fe(III) [2 × 2] grid complexes, with both HS and LS centers have been reported. Changing the sulfur atom to oxygen in L6c modulates the crystal field environment, and with $Fe(BF_4)_2$ in air the [2 × 2] grid $[Fe(II)_4(L6c)_4](BF_4)_4$ was obtained, which showed spin crossover behavior between 150 and 200 K associated with two adjacent iron centers, substantiated by structural data at both 123 and 283 K.[27a] The [2 × 2] grid complexes $[Fe(II)_4(L5b)_4](CF_3SO_3)_2$ and $[Fe(II)_4(L6b)_4]$ $(CF_3SO_3)_4$ have square μ-S and μ-O bridged square structures respectively, exhibiting LS diamagnetic behavior (2−300 K), and spin crossover of just one of the four HS Fe(II) center at ∼100 K respectively.[27b]

In the present study we report some iron complexes of the ligands poap, poapz, and the new hydrazone based ligands paox, phox, vaox, p2pyh, and p2ox (Chart 1). Examples of mononuclear Fe(III) complexes, dinuclear Fe(II) and Fe(III), and mixed oxidation state Fe(II)/Fe(III) complexes, tetranuclear [2 × 2] mixed oxidation state Fe(II)/Fe(III) grids, and a pentanuclear trigonal bipyramidal Fe(II) cluster complex are discussed. Structural and magnetic properties are presented and exchange contributions analyzed.

EXPERIMENTAL SECTION

Infrared spectra were recorded as Nujol mulls using a Mattson Polaris FT-IR instrument. Microanalyses were carried out by Canadian Microanalytical Service, Delta, Canada. Variable temperature magnetic data (2−300K) were obtained using a Quantum Design MPMS5S SQUID magnetometer using field strengths in the range 0.1 to 5 T. Background corrections for the sample holder assembly and diamagnetic components of the complexes were applied. Infrared spectra were obtained as Nujol mulls using a Mattson Polaris FT IR instrument. Mass spectra were obtained in methanol using an Agilent 1100 Series LC/MSD in APCI mode. NMR spectra were obtained with a Bruker 500 MHz instrument.

Synthesis of Ligands. The ligands poap,[10] poapz,[10] vaox,[28a] paox,[28b] and phox[28b] were synthesized according to published procedures.

p2ox. 2,6-Dicyanopyridine (0.37 g, 2.9 mmol) was added to a dilute solution of sodium methoxide in methanol (50 mL) and refluxed for 2 h. The resulting solution was adjusted to neutral pH with glacial acetic acid. 2-(Hydroxyimino)-propanehydrazone (HIPH)[28a,b] (0.80 g, 6.8 mmol) was added, and the resulting mixture was refluxed for 5 h and then stirred at room temperature (rt) for 48 h. The product, a pale yellow powder, was filtered and washed with excess methanol and ether. Yield (0.81 g, 81%). ^{1}H NMR (ppm, DMSO-d_6) 1.8 (s) (CH_3), 7.4−8.3 (m) (CH aromatic), 10 (s) (NH). ^{13}C NMR (ppm, DMSO-d_6): 10.14, 121.60, 137.14, 147.97, 149.20, 150.59, and 160.70. Selected IR data (Nujol, cm^{-1}): 3396, 3348, 1671, 1633, 1560, 1301, 721. Anal. Calcd. for $C_{13}H_{17}N_9O_4\cdot 3H_2O$: C, 37.39; H, 5.55; N, 30.21. Found: C, 37.81; H, 4.99; N, 30.36.

p2pyh. 2,6-Dicyanopyridine (0.35 g, 2.7 mmol) was added to a dilute solution of sodium methoxide in methanol (50 mL) and refluxed for 2 h. The resulting solution was adjusted to neutral pH with glacial acetic acid. Pyridine-2-carbohydrazide (0.82 g, 6.0 mmol) was added, and the resulting mixture was refluxed for 5 h and then stirred at rt for 48 h. The product, a pale yellow powder, was filtered off and washed with excess methanol and ether. Yield (0.80 g, 73%). ^{1}H NMR (ppm, DMSO-d_6) 7.5−8.8 (m) (CH aromatic), 10.7 (s) (NH). ^{13}C NMR (ppm, DMSO-d_6): 121.85, 122.28, 126.51, 137.50, 137.92, 148.39, 148.79, 149.35, 150.17, and 160.25. Selected IR data (Nujol, cm^{-1}): 3394, 3340, 1693, 1656, 1587, 1571, 1294, 721. Anal. Calcd. for $C_{19}H_{17}N_9O_2\cdot H_2O$: C, 54.13; H, 4.54; N, 29.92. Found: C, 54.75; H, 4.13; N, 30.10.

Synthesis of Complexes. *$[(poap)_4Fe_4Cl_4]Cl_2(CH_3OH)_8(H_2O)$ (1).* The ligand poap (0.06 g, 0.25 mmol) and $FeCl_2\cdot 4H_2O$ (0.20 g, 1.0 mmol) were stirred together in 5 mL of MeOH under nitrogen for 5 min. Dark red crystals appeared in 24 h (Yield 0.055 g; 13%), suitable for structural determination. IR data (Nujol, cm^{-1}): 3320, 1650, 1559, 1304, 1150, 1048, 1015, 797, 718. Anal. Calcd. for

dx.doi.org/10.1021/ic201891h | Inorg. Chem. 2011, 50, 12141−12154

$(C_{12}H_{10}N_5O)_4Fe_4Cl_6{\cdot}10H_2O$: C, 36.59; H, 3.84; N, 17.79. Found: C, 36.56; H, 3.04; N, 17.74.

[(poapz)$_6$Fe$_5$](CF$_3$SO$_3$)$_4$·7H$_2$O (**2**). A mixture of poapz (0.35 g, 1.4 mmol), $Fe(CF_3SO_3)_2{\cdot}(MeCN)_2$ (0.74 g, 1.5 mmol), and NaOAc (0.15 g, 1.8 mmol) was refluxed in 25 mL of dry MeOH under nitrogen for 16 h. The resulting solution was then filtered and left undisturbed. Dark almost black crystals appeared after several days (Yield 0.12 g; 35%). IR data (Nujol, cm^{-1}): 3250, 1652, 1300, 1029, 722. Anal. Calcd. for $[(C_{11}H_9N_6O)_6Fe_5](CF_3SO_3)_4{\cdot}7H_2O$ (**5**): C, 34.31; H, 2.78; N, 20.59. Found: C, 34.43; H, 2.46; N, 20.59.

[(paox)$_4$Fe$_4$Cl$_4$]Cl$_2$(CH$_3$OH)$_6$(H$_2$O) (**3**). The ligand paox (0.050 g, 0.24 mmol) and $FeCl_2{\cdot}4H_2O$ (0.21 g, 1.0 mmol) were stirred together in 5 mL of MeOH under nitrogen for 5 min, and the reaction flask was sealed. Dark red crystals appeared in 24 h (Yield 0.044 g; 13%), suitable for structural determination. IR data (Nujol, cm^{-1}): 3150, 1649, 1563, 1304, 1172, 1052, 1016, 916, 793, 749, 722. Anal. Calcd. for $(C_9H_9N_5O_2)_4Fe_4(Cl)_6{\cdot}13H_2O$: C, 27.97; H, 4.04; N, 18.13. Found: C, 27.90; H, 3.30; N, 18.13.

[(paox)$_4$Fe$_4$Cl$_4$](FeCl$_4$)$_2$(CH$_3$OH)$_2$ (**3a**). The ligand paox (0.050 g, 0.24 mmol) and $FeCl_3{\cdot}6H_2O$ (0.21 g, 0.74 mmol) were stirred together in 20 mL of MeOH for 30 min, without excluding air. The dark solution was then filtered, and the filtrate layered with ether. Dark red crystals appeared after 1 week (Yield 0.044 g; 13%) suitable for structural determination. IR data (Nujol, cm^{-1}): 3250, 1649, 1562, 1306, 1170, 1054, 721. Anal. Calcd. for $(C_9H_9N_5O_2)_4Fe_4Cl_4]$-$(FeCl_4)_2{\cdot}3H_2O{\cdot}CH_3OH$: C, 25.84; H, 2.67; N, 16.29. Found: C, 25.82; H, 2.65; N, 15.95.

[(paox)$_4$Fe$_4$(H$_2$O)$_2$(CH$_3$CN)$_2$](ClO$_4$)$_6$ (**4**). The ligand paox (0.050 g, 0.23 mmol), $Fe(ClO_4)_2{\cdot}6H_2O$ (0.20 g, 0.78 mmol), and L-ascorbic acid (0.050 g, 0.28 mmol) were stirred together in 10 mL of MeCN under nitrogen. The reaction mixture was stirred for 5 min and then filtered. The filtrate was left undisturbed for crystallization. Dark red crystals appeared after several days (Yield 0.035 g, 8.5%). IR data (Nujol, cm^{-1}): 1660, 1569, 1305, 1200, 1150, 1085, 721. Anal. Calcd. for $(C_9H_{10}N_5O_2)_4Fe_4(ClO_4)_6{\cdot}20H_2O$: C, 20.99; H, 3.88; N, 13.60. Found: C, 20.97; H, 3.05; N, 13.66.

[(phox)$_2$Fe$_2$Cl$_4$] (**5**). The ligand phox (0.050 g, 0.25 mmol) and $FeCl_3{\cdot}6H2O$ (0.20 g, 0. 74 mmol) were stirred together in 20 mL of MeOH. The reaction mixture was stirred for a further 30 min, and the solution filtered. The filtrate was left undisturbed for crystallization. A small quantity of dark red crystals appeared after several days (Yield ~4 mg). IR data (Nujol, cm^{-1}): 3304, 1649, 1616, 1520, 1294, 1120, 1157, 1026, 931, 897, 777, 737. Anal. Calcd. for $(C_9H_9N_4O_2)_2Fe_2(Cl)_4$: C, 32.62; H, 2.71; N, 16.91. Found: C, 32.55; H, 2.94; N, 16.60. The same complex is also produced by the reaction of $FeCl_2{\cdot}4H_2O$ and phox in the presence of ascorbic acid (Yield: 18%), and this sample was used for the magnetic study (vide infra).

[(vaox)$_2$Fe](CF$_3$SO$_3$)(CH$_3$OH)$_2$ (**6**). The ligand vaox (0.050 g, 0.20 mmol) and $Fe(CF_3SO_2)_2{\cdot}(MeCN)_2$ (0.21 g, 1.0 mmol) were stirred together in 5 mL of MeOH under nitrogen for 5 min. Dark red crystals appeared after 24 h (Yield 0.018 g; 12%) suitable for structural determination. IR data (Nujol, cm^{-1}): 3300, 1602, 1572, 1547, 1298, 1250, 1219, 1084, 1054, 1028, 722. Anal. Calcd. for $(C_{11}H_{11}N_3O_4)_2$ $Fe(CF_3SO_3){\cdot}2H_2O$: C, 37.34; H, 3.54; N, 11.36. Found: C, 37.85; H, 3.53; N, 11.45.

[(vaox)$_2$Fe$_2$Cl$_2$(CH$_3$OH)$_2$] (**7**). 2-(Hydroxyimino)-propanehydrazone (0.070 g, 0.60 mmol) and *o*-Vanillin (0.10 g, 0.65 mmol) were mixed together in 20 mL of MeOH to generate vaox in situ. Triethylamine (2 mL) was then added, and the reaction mixture was stirred for 10 min. $FeCl_2{\cdot}H_2O$ (0.13 g, 0.65 mmol) was added to the reaction mixture, which was stirred for a further 5 min and then filtered. Dark red crystals appeared in 24 h (Yield 0.050 g; 11%) suitable for structural determination. IR data (Nujol, cm^{-1}): 3165, 1608, 1563, 1297, 1252, 1223, 1200, 1109, 1079, 1004, 968, 921, 743, 720. Anal. Calcd. for $(C_{11}H_{11}N_3O_4)_2Fe_2Cl_2{\cdot}(CH_3OH)_2$: C, 38.70; H, 4.06; N, 11.29. Found: C, 38.77; H, 4.11; N, 11.34.

[(p2pyh)Fe(H$_2$O)$_2$](NO$_3$)$_3$(H$_2$O) (**8**). The ligand p2pyh (0.050 g, 0.12 mmol) and $Fe(NO_3)_3{\cdot}9H_2O$ (0.19 g, 0.47 mmol) were stirred together in 20 mL of MeOH. The reaction mixture was filtered, and the filtrate was left undisturbed for crystallization. Dark red crystals appeared after a few days (Yield 0.018 g; 12%). IR data (Nujol, cm^{-1}): 3381, 1712, 1669, 1649, 1577, 1301, 1227, 1038, 827, 752, 720. Anal. Calcd. for $[(C_{19}H_{16}N_9O_2)Fe(H_2O)_2]{\cdot}(NO_3)_3(H_2O)$: C, 32.66; H, 3.15; N, 24.06. Found: C, 32.01; H, 3.19; N, 23.61.

[(p2ox)Fe$_2$Cl$_3$(CH$_3$OH)$_2$](CH$_3$OH) (**9**). The ligand p2ox (0.030 g, 0.082 mmol) and $FeCl_2{\cdot}4H_2O$ (0.14 g, 0.70 mmol) were stirred together in 5 mL of MeOH under nitrogen for 5 min. Dark red crystals appeared after a few days (Yield 0.012 g, 24%) . IR data (Nujol, cm^{-1}): 3400, 2725, 1709, 1660, 1642, 1569, 1305, 1200, 1152, 721. Anal. Calcd. for $(C_{13}H_{16}N_9O_4)Fe_2(Cl)_3(CH_3OH)]{\cdot}2H_2O$: C, 25.96; H, 3.70; N, 19.47. Found: C, 25.44; H, 3.21; N, 19.81.

X-ray Crystallography. Crystals of **1**−**9** were mounted on low temperature diffraction loops and measured on a Rigaku Saturn CCD area detector with graphite monochromated Mo−Kα radiation. Structures were solved by direct methods[29,30] and expanded using Fourier techniques.[31] Neutral atom scattering factors were taken from Cromer and Waber.[32] Anomalous dispersion effects were included in Fcalc;[33] the values for $\Delta f'$ and $\Delta f''$ were those of Creagh and McAuley.[34] The values for the mass attenuation coefficients are those of Creagh and Hubbell.[35] All calculations were performed using the CrystalStructure[36,37] crystallographic software package except for refinement, which was performed using SHELXL-97.[29] Non-hydrogen atoms were refined anisotropically, while hydrogen atoms were introduced in calculated positions and refined on a riding model, unless otherwise indicated.

For **3**, **5**, **6**, **8**, and **9** collection, solution and refinement proceeded normally. For **3** lattice solvent (water and methanolic) protons could not be located from difference maps and were therefore omitted from the model, but included in the formula for the calculation of intensive properties. For **4**, **5**, **6**, **8**, and **9** O−H and N−H protons were located in difference map positions and refined positionally with distance restraints and isotropic displacement ellipsoids fixed at 1.2 or 1.5 times that of their bonding partners.

For **1**, the Platon[38] SQUEEZE procedure was applied to recover 791 electrons per unit cell in two voids (total volume 2699 Å^3); that is, 197.75 electrons per formula unit. Disordered solvent lattice methanol molecules were present prior to the application of SQUEEZE; however, a satisfactory point atom model could not be achieved. The application of Squeeze gave a good improvement in the data statistics and allowed for a full anisotropic refinement of the structure.

For **2**, crystals of this compound were prepared numerous times; however, they consistently diffracted too weakly, and decomposed too quickly, for the successful collection of a full data set. While the refinement values are far from ideal, this structure is presented in the context of other supporting experimental information. Protons could not be located in difference map positions for the lattice solvent water and methanol molecules and were omitted from the model; however, these protons were included in the formula for the calculation of intensive properties. All non-hydrogen atoms were refined anisotropically.

For **4**, Platon's[38] ADDSYM detected a (pseudo) center of symmetry; however, Platon's SPGRfromEX indicated that the two possible space groups based on systematic absences were *Pca*21 and *Pbcn*, with the probability of *Pca*21/*Pbcn* = 71. The structure was therefore refined in *Pca*21. Further, a solution could not be achieved in *Pbcn*. SHELXL MERG 4 was used, and the absolute structure was not determined. Note, however, that the Bayesian[39] statistics indicate that this is an inversion twin (P3(racemic twin) = 1.0000; Hooft y = 0.511(3)).

For **3a** and **7**, multiple crystals were collected; however, each diffracted very poorly. For **3a**, SHELXL ISOR restraints were applied to the lattice solvent methanol molecules. The hydroxy protons for the lattice methanol molecules could not be located in difference map positions and were omitted from the model, but included in the formula for the calculation of intensive properties. The occupancies of a disordered $[FeCl_4]^-$ were refined. For **7**, both Rigaku's[40] TwinSolve and Platon's[38] TwinRotMap were used to eliminate the possibility that the poor refinement values were due to missed twinning. Platon's[38] ADDSYM and SPGRfromEX were both employed to ensure that the space group was properly assigned. Four hydroxy H-atoms are missing

from the model, but have been included in the formula for the calculation of intensive properties.

RESULTS AND DISCUSSION

Structural Descriptions. *[(poap)$_4$Fe$_4$Cl$_4$]Cl$_2$·(CH$_3$OH)$_8$(H$_2$O) (**1**).* Crystal data for **1** are summarized in Table 1, and important bond distances and angles are listed in Table 2. The complex structure is shown in Figure 1 and consists of a [2 × 2] square grid with the four Fe centers bridged by μ-O hydrazone oxygen atoms, and with four ligands arranged in two directionally opposed parallel groups above and below the metal pseudoplane. Each ligand fills five coordination sites, and the four remaining sites at two Fe centers are occupied by chlorine ligand atoms. Bond Valence Sum (BVS)[41] calculations for Fe1 and Fe4 (1.97) and Fe2 and Fe3 (3.00) indicate that these pairs of centers are consistent with HS Fe(II) and HS Fe(III), respectively. This is also expected based on the coordination environments at these sites ($N_2O_2Cl_2$ vs N_4O_2). Fe−O−Fe bridge angles fall in the range 131−132°, and Fe−Fe distances fall in the range 3.85−3.88 Å. This is the first example of a [2 × 2] grid with this type of ligand, based on four Fe centers, although numerous examples with Mn(II), Co(II), Ni(II), Cu(II) are known.[10,11]

*[(poapz)$_6$Fe$_5$](CF$_3$SO$_3$)$_4$·7H$_2$O (**2**).* Crystal data for **2** are summarized in Table 1, and important bond distances and angles are listed in Table 3. **2** has a rare homoleptic pentanuclear cationic structure, with the pentanuclear metal core surrounded by six ligands as shown in Figure 2. The metal based polyhedron is a trigonal bipyramid, with the six ditopic poapz ligands completing all the coordination sites of the five six-coordinate metal ions. A core structure is shown in Figure 3 to illustrate the simple μ-O bridging arrangement. This type of homoleptic cluster has been observed before with ditopic pyridine hydrazone ligands, but only seems to occur when the anion has weak coordinating capacity, as in the present case. Other isostructural examples have been observed with Mn(II), Co(II), and Zn(II).[42,43] The apical Fe centers are bridged to the three equatorial Fe centers via μ-O linkages, typical of the bridging action of such ligands in square [2 × 2] tetranuclear complexes. The apical Fe centers have N_3O_3 coordination spheres, and the equatorial atoms have N_4O_2 coordination spheres. Fe-ligand distances are typical of iron in a +2 state (BVS values Fe1 = 2.02, Fe2 = 1.98, Fe3 = 2.05, Fe4 = 2.03, Fe5 = 2.09). Fe−O−Fe angles fall in the range 130−134°, typical of this sort of μ-O bridging arrangement, suggesting intramolecular antiferromagnetic exchange (vide infra).

*[(paox)$_4$Fe$_4$Cl$_4$]Cl$_2$(CH$_3$OH)$_6$(H$_2$O) (**3**).* Crystal data for **3** are summarized in Table 1, and important bond distances and angles are listed in Table 4. **3** has a square [2 × 2] grid structure, shown in Figure 4, and is similar to **1** with four ligands arranged in an opposed orientation on either face of the square, and four μ-O hydrazone oxygen atoms bridging the four iron centers. Four chlorine atoms are coordinated to two iron centers (Fe2 and Fe4) in a *cis*-fashion. Terminal pyridine nitrogen atoms coordinate at one ligand end, while only the oxime nitrogen atom is involved in coordination at the other end. The close proximity of the Cl ligands (Cl1−Cl4) and the adjacent oxime hydrogen atoms suggests that there are Cl−H hydrogen bonding contacts, which may contribute to the particular arrangement of the ligands and chlorine atoms within the square grid. Metal−ligand bond lengths at Fe1 and Fe3 (BVS values of 2.94, 2.93 respectively) are much shorter than those at Fe2 and Fe4 (BVS values of 2.07, 2.11 respectively), indicating that Fe1 and Fe3 are HS Fe(III) sites, and Fe2 and Fe4 are HS Fe(II) sites. This would agree with the charge balance based on the presence of six chlorine atoms, and four ligands with a −1 charge due to hydrazone oxygen proton loss. The Fe−O−Fe bridge angles fall in the range 129.8−132.4°, and Fe−Fe distances in the range 3.798−3.881 Å (ave. 3.855 Å). The relative arrangement of the Fe(II) and Fe(III) sites is the same as in **1**. In both cases the complex ends up with the same oxidation state situation, despite starting with Fe(II), and the apparently preferred arrangement of Fe(II) and Fe(III) sites agrees with the respective ligand environments. The oxidation of the two iron sites presumably results from some exposure of the system to some air during synthesis and workup.

*[(paox)$_4$Fe$_4$Cl$_4$][FeCl$_4$]$_2$(CH$_3$OH)$_2$ (**3a**).* **3a** contains a [2 × 2] grid cation and two $[Fe(III)Cl_4]^-$ counterions, giving an overall charge balance which indicates the presence of two Fe(II) and two Fe(III) sites in the grid. Crystal data for **3a** are summarized in Table 1, and important bond distances and angles are listed in Supporting Information, Table S1. The structure of the cation itself is essentially identical to that in **3**, and is shown in Supporting Information, Figure S1. Fe2 and Fe4 have longer average bond distances (BVS 2.09, 2.19 respectively) than Fe1 and Fe3 (3.05, 3.12 respectively) indicating Fe(II) and Fe(III) sites, respectively. The Fe5 counterion is tetrahedral (BVS 3.17), confirming Fe(III). The other $FeCl_4^-$ site is disorded over two positions. Fe−O−Fe bridge angles within the grid fall in the range 130.4−131.5°, similar to those in **3**, and Fe−Fe distances in the range 3.818−3.828 Å (ave. 3.824 Å), indicating a very similar overall arrangement of the metal ions in the two different oxidation states and the ligands. What distinguishes the two cases (**3** and **3a**) is clearly the fact that for **3** Fe(II) starting material was used, while for **3a** the starting material was Fe(III) (vide infra).

*[(paox)$_4$Fe$_4$(H$_2$O)$_2$(CH$_3$CN)$_2$](ClO$_4$)$_6$ (**4**).* Crystal data for **4** are summarized in Table 1, and important bond distances and angles are listed in Table 5. **4** has a square [2 × 2] grid structure, shown in Figure 5, with four ligands arranged in an opposed orientation on either face of the square, and four μ-O hydrazone oxygen atoms bridging the four iron centers. It is very similar to the overall structure of **3**, but differs in the coligand complement. The four coordination sites left empty by the coordination of the four ligands are occupied by two water molecules, and two acetonitrile molecules. The six perchlorate anions are uncoordinated. The charge balance indicates that, on the assumption that each paox ligand bears a −1 charge, two of the iron centers are Fe(II) and two are Fe(III). Relatively long bond distances at Fe1 and Fe4 (ave. 2.139, 2.136 Å respectively), and much shorter distances at Fe2 and Fe3 (ave. 2.071, 2.065 Å respectively), point to HS Fe(II) and Fe(III) sites respectively. This is supported by the corresponding BVS values (2.10, 2.12 and 2.89, 2.97, respectively). Fe−O−Fe angles fall in the range 131.0−132.6°, and Fe−Fe distances in the range 3.79−3.84 Å.

*[(phox)$_2$Fe$_2$Cl$_4$] (**5**).* Crystal data for **5** are summarized in Table 1, and important bond distances and angles are listed in Table 6. The structure of **5** is dinuclear, in contrast to that of **4**, and is shown in Figure 6, panels a and b. Half of the molecule is contained in the asymmetric unit, with the Fe center in a distorted square pyramidal environment (Figure 6a), with a chlorine ligand, and phox bound via N_2O coordination, in the basal plane. Fe−N distances fall in the range 2.11−2.18 Å, with a Fe−Cl distance of 2.382(2) Å. A slightly longer axial Fe−Cl

dx.doi.org/10.1021/ic201891h | Inorg. Chem. 2011, 50, 12141−12154

Table 1. Summary of Crystallographic Data for 1−9

	1	2	3	3a
chemical formula	$C_{59}H_{84}Cl_6Fe_4N_{20}O_{15}$	$C_{72}H_{78}F_{12}Fe_5N_{36}O_{25}S_4$	$C_{42}H_{66}Cl_6Fe_4N_{20}O_{15}$	$C_{40}H_{56}Cl_{12}Fe_6N_{20}O_{12}$
M	1749.54	2483.09	1527.21	1769.53
T (K)	163(2)	123(2)	158(2)	158(2)
crystal system	monoclinic	triclinic	triclinic	monoclinic
space group	$P2_1/c$ (#14)	$P\bar{1}$ (#2)	$P\bar{1}$ (#2)	$P2_1/a$ (#14)
a (Å)	15.692(5)	14.235(5)	12.7241(12)	14.5433 (12)
b (Å)	29.941(8)	14.512(6)	14.1843(12)	37.143(3)
c (Å)	21.670(7)	26.039(1)	20.880(2)	15.2818(14)
α (deg)	90.00	99.829(7)	74.137(5)	90.00
β (deg)	130.817(4)	93.742(7)	80.594(6)	117.171(5)
γ (deg)	90.00	99.903(7)	70.854(5)	90.00
V (Å^3)	7705(4)	5196(3)	3413.1(5)	7344.0(10)
Z	4	2	2	4
D_{calc} (g/cm^3)	1.508	1.587	1.486	1.600
μ(MoKα) (cm^{-1})	10.19	8.70	11.37	16.51
reflections total	92295	38706	33142	13057
reflections unique ($I > 2.00\sigma(I)$)	12939	15080	12298	10099
R_{int}	0.0700	0.0430	0.0376	0.0491
R_1 ($I > 2.00\sigma(I)$)	0.0895	0.1659	0.0791	0.1160
wR_2 (All reflections)	0.2818	0.4705	0.2417	0.2774
	4	**5**	**6**	**7**
chemical formula	$C_{44}H_{56}Cl_6Fe_4N_{24}O_{34}$	$C_{18}H_{20}Cl_4Fe_2N_8O_4$	$C_{25}H_{32}F_3FeN_6O_{13}S$	$C_{24}H_{30}Cl_2Fe_2N_6O_{10}$
M	1901.17	665.91	769.46	745.14
T (K)	163(2)	163(2)	163(2)	173(2)
crystal system	orthorhombic	monoclinic	triclinic	triclinic
space group	$Pca2_1$ (#29)	$C2/c$ (#15)	$P\bar{1}$ (#2)	$P\bar{1}$ (#2)
a (Å)	18.5879(18)	18.705(4)	10.936(5)	7.58(2)
b (Å)	18.1873(17)	10.8869(17)	12.166(5)	8.79(3)
c (Å)	24.891(2)	13.453(3)	13.613(6)	11.16(4)
α (deg)	90.00	90.00	98.001(4)	102.98(6)
β (deg)	90.00	113.481(11)	109.712(5)	100.03(4)
γ (deg)	90.00	90.00	96.538(4)	92.09(7)
V (Å^3)	8414.7(13)	2512.8(8)	1663.1(13)	711(4)
Z	4	4	2	1
D_{calc} (g/cm^3)	1.501	1.760	1.536	1.740
μ(MoKα) (cm^{-1})	9.58	16.22	6.04	12.76
reflections total	72915	4037	14963	3939
reflections unique ($I > 2.00\sigma(I)$)	8692	2235	6578	1927
R_{int}	0.0463	0.0662	0.0318	0.0807
R_1 ($I > 2.00\sigma(I)$)	0.0641	0.0782	0.0441	0.1415
wR_2 (All reflections)	0.1849	0.2094	0.1564	0.3495
		8		**9**
chemical formula		$C_{19}H_{23}FeN_{12}O_{14}$		$C_{16}H_{27}Cl_3Fe_2N_9O_7$
M		699.31		675.50
T (K)		163(2)		163(2)
crystal system		triclinic		monoclinic
space group		$P\bar{1}$ (#2)		$P2_1/c$ (#14)
a (Å)		7.644(4)		15.649(3)
b (Å)		13.564(8)		12.014(2)
c (Å)		14.095(8)		13.890(3)
α (deg)		102.025(4)		90.00
β (deg)		99.522(7)		89.960(3)
γ (deg)		100.715(7)		90.00
V (Å^3)		1372.4(13)		2611.4(9)
Z		2		4
D_{calc} (g/cm^3)		1.692		1.718
μ(MoKα) (cm^{-1})		6.43		14.73
reflections total		12678		14862
reflections unique ($I > 2.00\sigma(I)$)		5331		4928
R_{int}		0.0503		0.0304
R_1 ($I > 2.00\sigma(I)$)		0.0505		0.0386
wR_2 (all reflections)		0.1291		0.0984

dx.doi.org/10.1021/ic201891h | Inorg. Chem. 2011, 50, 12141−12154

Table 2. Selected Distances (Å) and Angles (deg) for 1

Distances	
Fe1−N1	2.180(3)
Fe1−N11	2.193(3)
Fe1−O1	2.222(2)
Fe1−O3	2.225(2)
Fe1−Cl1	2.3895(10)
Fe1−Cl2	2.4265(10)
Fe2−N18	2.006(3)
Fe2−N3	2.007(3)
Fe2−O4	2.021(2)
Fe2−O1	2.022(2)
Fe2−N5	2.157(3)
Fe2−N20	2.162(3)
Fe3−N16	2.174(3)
Fe3−N6	2.182(3)
Fe3−O4	2.209(2)
Fe3−O2	2.237(2)
Fe3−Cl4	2.3823(10)
Fe3−Cl3	2.4304(10)
Fe4−N8	2.010(3)
Fe4−N13	2.011(3)
Fe4−O3	2.018(2)
Fe4−O2	2.021(2)
Fe4−N10	2.172(3)
Fe4−N15	2.176(3)
Angles	
Fe2−O1−Fe1	131.27(11)
Fe4−O2−Fe3	131.03(11)
Fe4−O3−Fe1	130.59(12)
Fe2−O4−Fe3	131.47(11)

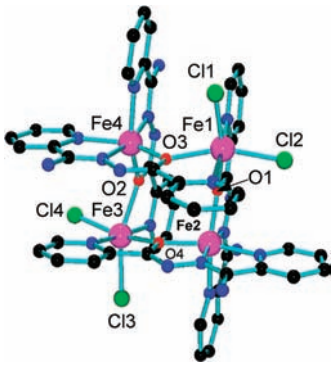

Figure 1. Structural representation for **1**.

bond distance (2.401 Å) completes the square pyramid. The main distortion occurs through a bend in the O1−Fe1−N1 basal pair of bonds (146.8°), resulting from the chelating effect of phox, and the formation of two adjacent five-membered chelate rings. The oxime end-piece remains uncoordinated. Relatively long bond distances indicate the iron centers are in the +2 oxidation state (BVS value 2.07).[41] The two halves of the dimer are linked by two chlorine bridges through Cl1 in an unusual asymmetric arrangement, with a very long symmetry imposed Fe1−Cl1 bridging distances (2.648(2) Å). The Cl1−Fe−Cl1′ bridge angle is 96.17(5)°. This type of asymmetric (long−short) chlorine bridging situation has been observed before in comparable dinuclear Fe(II) dimeric complexes.[44,45]

[(vaox)$_2$Fe](CF$_3$SO$_3$)(CH$_3$OH)$_2$ (***6***). Crystal data for **6** are summarized in Table 1, and important bond distances and angles are listed in Table 7. **6** has a mononuclear structure (Figure 7), with two ligands bound through NO_2 meridional

Table 3. Selected Distances (Å) and Angles (deg) for 2

Distances	
Fe1−O4	2.065(5)
Fe1−O6	2.081(5)
Fe1−O1	2.108(5)
Fe1−N1	2.135(7)
Fe1−N31	2.164(6)
Fe1−N19	2.183(6)
Fe2−N3	2.072(7)
Fe2−N15	2.097(7)
Fe2−O3	2.126(5)
Fe2−O1	2.168(5)
Fe2−N18	2.259(6)
Fe2−N6	2.278(6)
Fe3−O3	2.099(5)
Fe3−O2	2.099(5)
Fe3−N25	2.135(6)
Fe3−O5	2.150(5)
Fe3−N13	2.165(7)
Fe3−N7	2.177(6)
Fe4−N33	2.071(6)
Fe4−N9	2.072(6)
Fe4−O2	2.112(5)
Fe4−O6	2.157(5)
Fe4−N12	2.221(7)
Fe4−N36	2.233(6)
Fe5−N27	2.062(5)
Fe5−N21	2.071(6)
Fe5−O4	2.149(5)
Fe5−O5	2.151(5)
Fe5−N24	2.223(7)
Fe5−N30	2.300(6)
Angles	
Fe1−O1−Fe2	131.6(2)
C17−O2−Fe3	116.9(4)
C17−O2−Fe4	111.4(4)
Fe3−O2−Fe4	130.4(2)
C28−O3−Fe3	116.4(5)
C28−O3−Fe2	112.2(4)
Fe3−O3−Fe2	130.6(3)
C39−O4−Fe1	117.7(5)
C39−O4−Fe5	110.6(5)
Fe1−O4−Fe5	130.6(2)
C50−O5−Fe3	114.8(4)
C50−O5−Fe5	111.3(4)
Fe3−O5−Fe5	132.9(2)
C61−O6−Fe1	117.3(4)
C61−O6−Fe4	110.8(4)
Fe1−O6−Fe4	130.5(2)

coordination to a six-coordinate iron center. Short average Fe−L distances (2.034 Å), and a BVS value of 3.07 indicate that iron is in the +3 oxidation state. One triflate anion is found in the lattice, indicating that each ligand bears a −1 charge. Short hydrazone CO bond distances (1.250(3) and 1.251(3) Å) indicate ketonic character, while longer CO distances in the vanillin phenolic group (1.322 Å) indicate proton loss at these sites. The vanillin MeO oxygen, and the oxime groups are not involved in coordination.

[(vaox)$_2$Fe$_2$Cl$_2$(CH$_3$OH)$_2$] (***7***). Crystal data for **7** are summarized in Table 1, and important bond distances and angles are listed in Table 8. A structural representation of **7** is shown in Figure 8, revealing that another coordination mode for vaox involves bridging through the hydrazone oxygen atom,

dx.doi.org/10.1021/ic201891h | *Inorg. Chem.* 2011, 50, 12141−12154

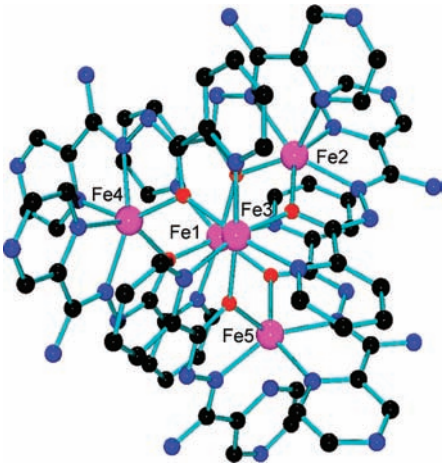

Figure 2. Structural representation for **2**.

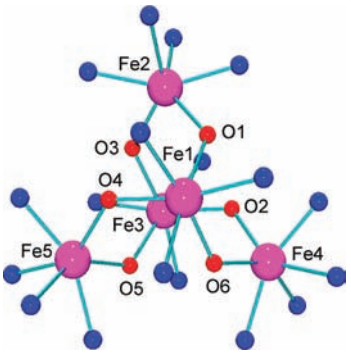

Figure 3. Structural representation for for the core in **2**.

Table 4. Selected Distances (Å) and Angles (deg) for 3

Distances	
Fe1–O5	2.013(3)
Fe1–N3	2.014(5)
Fe1–O1	2.015(3)
Fe1–N13	2.021(4)
Fe1–N11	2.152(4)
Fe1–N1	2.178(4)
Fe2–N5	2.127(4)
Fe2–N20	2.135(4)
Fe2–O7	2.213(3)
Fe2–O1	2.218(3)
Fe2–Cl2	2.4111(13)
Fe2–Cl1	2.4144(13)
Fe3–N8	2.007(4)
Fe3–N18	2.011(4)
Fe3–O7	2.030(3)
Fe3–O3	2.037(3)
Fe3–N16	2.153(4)
Fe3–N6	2.161(4)
Fe4–N10	2.133(4)
Fe4–N15	2.140(4)
Fe4–O5	2.181(3)
Fe4–O3	2.200(3)
Fe4–Cl4	2.3910(13)
Fe4–Cl3	2.4189(13)
Angles	
Fe1–O1–Fe2	132.37(16)
Fe3–O3–Fe4	131.72(16)
Fe1–O5–Fe4	129.75(16)
Fe3–O7–Fe2	132.33(15)

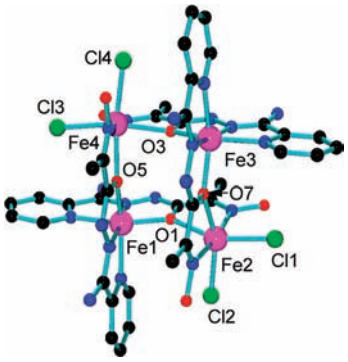

Figure 4. Structural representation for **3**.

Table 5. Selected Distances (Å) and Angles (deg) for 4

Distances	
Fe1–N21	2.111(7)
Fe1–O9	2.123(6)
Fe1–O1	2.132(4)
Fe1–N15	2.142(6)
Fe1–O5	2.162(4)
Fe1–N5	2.171(5)
Fe2–N3	2.012(5)
Fe2–N18	2.020(5)
Fe2–O7	2.041(4)
Fe2–O1	2.053(4)
Fe2–N1	2.144(5)
Fe2–N16	2.155(5)
Fe3–N13	1.987(5)
Fe3–N8	2.005(5)
Fe3–O5	2.029(4)
Fe3–O3	2.056(4)
Fe3–N6	2.146(5)
Fe3–N11	2.147(6)
Fe4–O10	2.101(5)
Fe4–O3	2.110(4)
Fe4–N20	2.139(5)
Fe4–N22	2.146(6)
Fe4–O7	2.150(4)
Fe4–N10	2.170(5)
Angles	
Fe2–O1–Fe1	132.0(2)
Fe3–O3–Fe4	131.2(2)
Fe3–O5–Fe1	132.8(2)
Fe2–O7–Fe4	132.7(2)

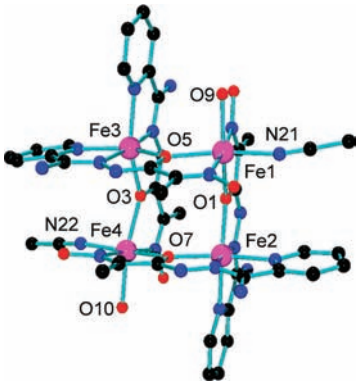

Figure 5. Structural representation for **4**.

with the formation of a dinuclear structure. Two seven-coordinate iron centers are connected by two μ_2-O bridging

dx.doi.org/10.1021/ic201891h | *Inorg. Chem.* 2011, 50, 12141–12154

Table 6. Selected Distances (Å) and Angles (deg) for 5

Distances	
Fe1−N2	2.111(5)
Fe1−O1	2.158(4)
Fe1−N1	2.176(5)
Fe1−Cl1	2.3817(15)
Fe1−Cl2	2.4015(17)
Fe1−Cl1	2.6483(17)
Cl1−Fe1	2.6482(17)
Angles	
N2−Fe1−O1	73.31(17)
N2−Fe1−N1	74.22(18)
O1−Fe1−N1	146.79(17)
N2−Fe1−Cl1	167.26(14)
O1−Fe1−Cl1	113.84(12)
N1−Fe1−Cl1	96.91(14)
N2−Fe1−Cl2	94.02(13)
O1−Fe1−Cl2	89.24(12)
N1−Fe1−Cl2	99.82(13)
Cl1−Fe1−Cl2	96.56(6)
N2−Fe1−Cl1	86.67(13)
O1−Fe1−Cl1	83.39(12)
N1−Fe1−Cl1	87.97(13)
Cl1−Fe1−Cl1	83.83(5)
Cl2−Fe1−Cl1	172.08(6)
Fe1−Cl1−Fe1	96.17(5)

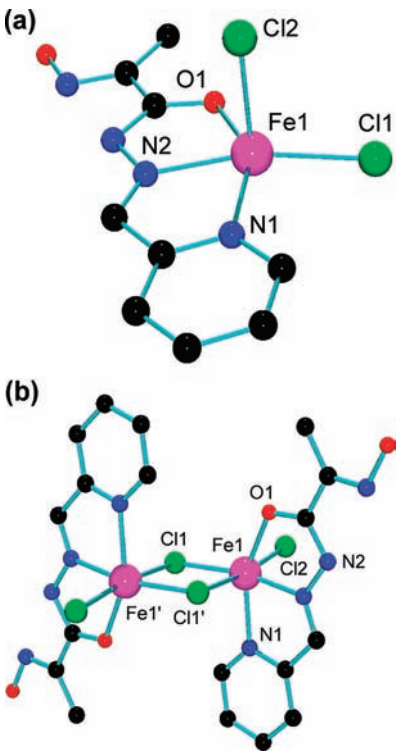

Figure 6. (a) Structural representation for asymmetric unit in **5**. (b) Dimeric structural representation for **5**.

ligands, with oxime N-coordination at one end, and NO_{phenol} coordination at the other end. Fe−ligand distances are relatively short (ave. 2.13 Å), indicating +3 oxidation states at the Fe centers (BVS 3.19), with an overall charge balance associated with each ligand losing two protons, in addition to the two chlorine ligands. The Fe−O−Fe bridge angles are 114.1°, and the metal ions are separated by 3.47 Å. In this case

Table 7. Selected Distances (Å) and Angles (deg) for 6

Distances	
Fe1−O5	1.8972(17)
Fe1−O1	1.9140(18)
Fe1−O7	2.0699(17)
Fe1−O3	2.0918(18)
Fe1−N4	2.1142(19)
Fe1−N1	2.119(2)
Angles	
O5−Fe1−O1	98.10(8)
O5−Fe1−O7	160.43(7)
O1−Fe1−O7	91.81(8)
O5−Fe1−O3	92.04(7)
O1−Fe1−O3	159.20(7)
O7−Fe1−O3	84.24(7)
O5−Fe1−N4	86.17(7)
O1−Fe1−N4	105.13(8)
O7−Fe1−N4	74.93(7)
O3−Fe1−N4	93.58(8)
O5−Fe1−N1	107.98(7)
O1−Fe1−N1	84.93(8)
O7−Fe1−N1	89.60(7)
O3−Fe1−N1	74.66(8)
N4−Fe1−N1	161.59(8)

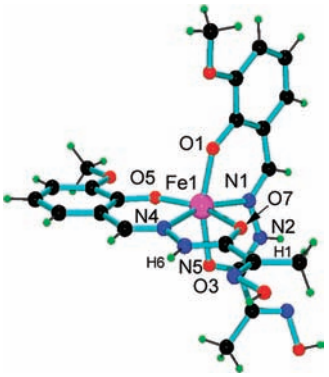

Figure 7. Structural representation for **6**.

the oxime groups are bound by nitrogen only, and as before the vanillin group only binds through the phenolic oxygen.

[(p2pyh)Fe(H$_2$O)$_2$](NO$_3$)$_3$(H$_2$O) (***8***). Crystal data for **8** are summarized in Table 1, and important bond distances and angles are listed in Table 9. A structural representation of **8** is shown in Figure 9. The ligand p2pyh is built on a central 2,6-pyridine core, and chelation at that group predisposes the coordination to the incorporation of just one metal ion. This occurs in **8**, with N_3O_2 in-plane coordination to the seven coordinate iron center. Two water molecules are bound at the axial sites. The external pyridine groups remain uncoordinated. The short overall Fe-ligand bond distances (ave. 2.12 Å) are consistent with Fe(III) in a seven coordinate environment (BVS 2.91).

[(p2ox)$_2$Fe$_2$Cl$_3$(CH$_3$OH)$_2$](CH$_3$OH) (***9***). Crystal data for **9** are summarized in Table 1, and important bond distances and angles are listed in Table 10. A structural representation of **9** is shown in Figure 10. The bis-oxime ligand coordinates in a bridging fashion, reminiscent of the situation in **7**, with the two iron centers bridged by hydrazone oxygen atoms. However, what is remarkable is that just one ligand encompasses the two metal ions, binding in a heptadentate fashion, but with the bridging action of the two hydrazone oxygen atoms it actually fills nine metal coordination sites. A single chlorine ligand binds

dx.doi.org/10.1021/ic201891h | Inorg. Chem. 2011, 50, 12141−12154

Table 8. Selected Distances (Å) and Angles (deg) for 7

Distances	
Fe1−O2	1.889(8)
Fe1−O3	2.035(8)
Fe1−O3	2.093(9)
Fe1−O5	2.107(7)
Fe1−N1	2.174(9)
Fe1−N3	2.289(8)
Fe1−Cl1	2.300(5)
Angles	
O2−Fe1−O3	150.8(3)
O2−Fe1−O3	140.7(2)
O3−Fe1−O3	65.7(2)
O2−Fe1−O5	89.5(3)
O3−Fe1−O5	80.6(3)
O3−Fe1−O5	83.5(3)
O2−Fe1−N1	81.3(4)
O3−Fe1−N1	71.3(3)
O3−Fe1−N1	137.1(3)
O5−Fe1−N1	90.0(3)
O2−Fe1−N3	74.2(3)
O3−Fe1−N3	132.4(3)
O3−Fe1−N3	67.0(3)
O5−Fe1−N3	88.4(3)
N1−Fe1−N3	155.4(3)
O2−Fe1−Cl1	99.4(3)
O3−Fe1−Cl1	91.8(3)
O3−Fe1−Cl1	89.0(2)
O5−Fe1−Cl1	170.97(18)
N1−Fe1−Cl1	92.3(3)
N3−Fe1−Cl1	93.1(3)
Fe1−O3−Fe1	114.3(2)

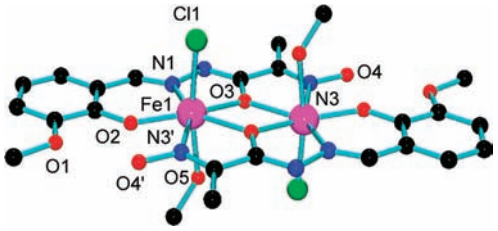

Figure 8. Structural representation for 7.

to Fe2, while two chlorine ligands bind to Fe1. The Fe−ligand bond distances at Fe1 (ave. 2.19 Å) are significantly shorter than at Fe2 (ave. 2.27 Å) (BVS values 3.05, 1.99 respectively) indicating that Fe1 is Fe(III) and Fe2 is Fe(II). This is remarkable, particularly since two chlorine ligands are bound to Fe1. However, the chelation effect at Fe1, combined with binding of the oxime ligand ends around Fe2, must create a tight coordination pocket, leading to a strong crystal field situation and stability of Fe(III). The Fe−O−Fe bridge angles are 111.9° and 113.0° at O6 and O7, respectively, and the Fe−Fe distance is 3.479 Å.

Redox Reactions. Iron coordination chemistry is much more complicated than that associated with most other transition metal ions, because of the propensity of iron to undergo redox reactions, and also to exhibit spin crossover properties. The stability of a particular oxidation state, and also spin state, is critically dependent upon the coordination environment available to the metal ion, and also the presence of potential oxidants and reductants. Oxygen is a principal reagent causing oxidation of Fe(II) to Fe(III), but because of the modest redox couple (Fe(III)/Fe(II) reduction potential

Table 9. Selected Distances (Å) and Angles (deg) for 8

Distances	
Fe1−O3	2.045(2)
Fe1−O4	2.048(2)
Fe1−O2	2.068(2)
Fe1−O1	2.1097(18)
Fe1−N3	2.129(2)
Fe1−N7	2.160(2)
Fe1−N5	2.260(2)
Angles	
O3−Fe1−O4	176.53(7)
O3−Fe1−O2	89.96(8)
O4−Fe1−O2	89.41(8)
O3−Fe1−O1	93.32(8)
O4−Fe1−O1	89.87(8)
O2−Fe1−O1	77.12(8)
O3−Fe1−N3	90.03(8)
O4−Fe1−N3	92.26(8)
O2−Fe1−N3	149.20(7)
O1−Fe1−N3	72.14(8)
O3−Fe1−N7	91.34(8)
O4−Fe1−N7	85.22(8)
O2−Fe1−N7	72.42(8)
O1−Fe1−N7	149.17(8)
N3−Fe1−N7	138.36(8)
O3−Fe1−N5	89.76(8)
O4−Fe1−N5	88.62(8)
O2−Fe1−N5	141.65(8)
O1−Fe1−N5	141.16(8)
N3−Fe1−N5	69.14(8)
N7−Fe1−N5	69.25(8)

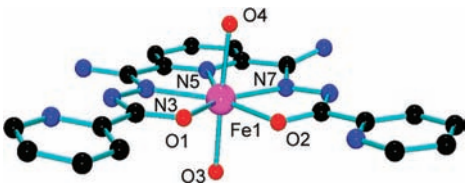

Figure 9. Structural representation for 8.

E^0 = 0.771 V), reduction of Fe(III) to Fe(II) might be anticipated as well. Air was excluded initially in most reactions and in one case (**4**) ascorbic acid was used in an attempt to stabilize the Fe(II) oxidation state.

For **1**, **3**, **4**, **6**, 7, and **9** oxidation of Fe(II) to Fe(III) occurred at some iron sites, which can be attributed to the adventitious presence of oxygen at some point during the syntheses. In the cases of **1**, **3**, and **4** the HS Fe(III) sites within the grids have N_4O_2 coordination spheres, while the HS Fe(II) sites have $N_2O_2Cl_2$ (**1**, **3**) and N_3O_3 (**4**) coordination spheres, with one acetonitrile bound to each Fe(II) in **4**. It is notable that the crystal field strength would differ considerably for these donor groupings and for the Fe(II) sites much weaker fields would be anticipated. In addition the coordinated CH_3CN in **4** would provide a reducing environment. Therefore it seems that a driving force for selective oxidation of Fe(II) is the ligand environment created by the congruence of the four ligands which assemble with four metal ions to form the grid. The heteroleptic nature of the assembly allows four extra ligands to coordinate, and exogenous groups available in the reaction mixtures bind to stabilize the Fe(II) sites. What is most remarkable is the case for **3a**, where the starting material was Fe(III). The same $Fe(II)_2Fe(III)_2$ grid assembly occurs as that

dx.doi.org/10.1021/ic201891h | Inorg. Chem. 2011, 50, 12141–12154

Table 10. Selected Distances (Å) and Angles (deg) for 9

Distances	
Fe1−O3	2.0130(16)
Fe1−O2	2.0242(16)
Fe1−N3	2.101(2)
Fe1−N6	2.1087(19)
Fe1−N12	2.1425(19)
Fe1−Cl1	2.4693(8)
Fe1−Cl2	2.4738(8)
Fe2−O2	2.1474(17)
Fe2−O5	2.159(2)
Fe2−O6	2.1728(19)
Fe2−O3	2.1851(16)
Fe2−Cl3	2.4047(8)
Fe2−N1	2.407(2)
Fe2−N8	2.427(2)
Angles	
O3−Fe1−O2	70.14(7)
O3−Fe1−N3	142.13(7)
O2−Fe1−N3	71.99(7)
O3−Fe1−N6	72.34(7)
O2−Fe1−N6	142.47(7)
N3−Fe1−N6	145.50(7)
O3−Fe1−N12	144.85(7)
O2−Fe1−N12	145.00(7)
N3−Fe1−N12	73.01(7)
N6−Fe1−N12	72.51(7)
O3−Fe1−Cl1	90.64(5)
O2−Fe1−Cl1	88.74(5)
N3−Fe1−Cl1	89.12(5)
N6−Fe1−Cl1	92.48(6)
N12−Fe1−Cl1	90.67(5)
O3−Fe1−Cl2	89.66(5)
O2−Fe1−Cl2	89.72(6)
N3−Fe1−Cl2	89.57(6)
N6−Fe1−Cl2	89.28(6)
N12−Fe1−Cl2	90.09(5)
Cl1−Fe1−Cl2	178.23(2)
O2−Fe2−O5	85.75(8)
O2−Fe2−O6	84.50(7)
O5−Fe2−O6	168.57(8)
O2−Fe2−O3	64.74(6)
O5−Fe2−O3	82.33(8)
O6−Fe2−O3	88.11(7)
O2−Fe2−Cl3	149.95(5)
O5−Fe2−Cl3	96.08(7)
O6−Fe2−Cl3	95.35(5)
O3−Fe2−Cl3	145.29(5)
O2−Fe2−N1	65.22(6)
O5−Fe2−N1	90.07(8)
O6−Fe2−N1	91.25(7)
O3−Fe2−N1	129.78(7)
Cl3−Fe2−N1	84.76(5)
O2−Fe2−N8	128.54(6)
O5−Fe2−N8	94.30(8)
O6−Fe2−N8	87.15(7)
O3−Fe2−N8	64.30(6)
Cl3−Fe2−N8	81.35(5)
N1−Fe2−N8	165.80(7)
Fe1−O2−Fe2	113.00(8)
Fe1−O3−Fe2	111.88(7)

in **3**, highlighting the obvious stabilizing effects associated with the particular combinations of donors at the four metal sites. In this case reduction, rather than oxidation, clearly occurs.

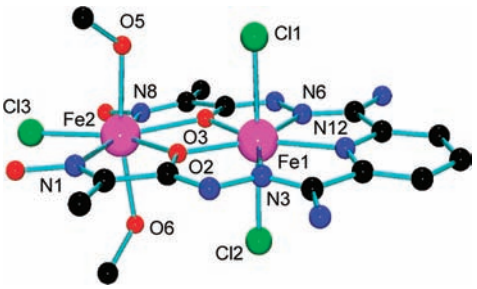

Figure 10. Structural representation for **9**.

The ligands themselves are built on hydrazone cores, and it is reasonable to assume that at some point in the reaction ligand hydrolysis has occurred, presumably induced by the polarizing effect of Fe(III) coordinated to the hydrazone imine nitrogen producing the corresponding amidrazone, which would have reducing potential. No ligand byproducts were detected in the reaction mixture.

The oxidations of Fe(II) in **6** and **7** produced just Fe(III) products, but for **9** once again a mixed oxidation state complex results. In this case the Fe(II) site is created by the weaker ligand field associated with the loose fit of the metal ion in the strained end pocket of the complex. Complex **5** is perhaps the most remarkable, since it contains two Fe(II) sites, starting with Fe(III). Clearly the chlorine rich nature of the coordination sphere must exert a dominant influence in this case, helping to stabilize Fe(II). However, once again imine hydrolysis would reasonably be the source of reducing equivalents, and in the case of phox, derived from pyridine-2-carboxaldehyde, this is perhaps not surprising.

Magnetic Studies. Variable temperature magnetic data for **1** are shown in Figure 11. The moment per mole drops from

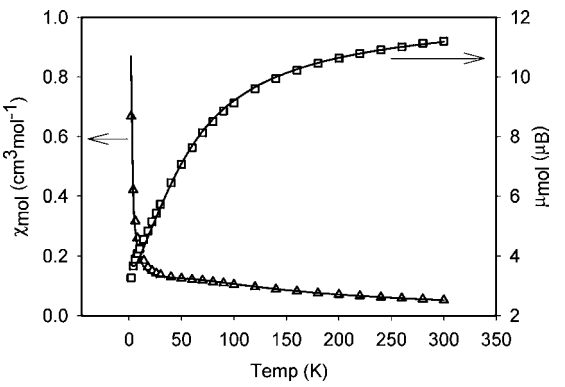

Figure 11. Variable temperature magnetic data for **1**. See text for fitted parameters.

11.2 μ_B at 300 K to 3.27 μ_B at 2 K. The rt value is consistent with the sum of two HS Fe(II) and two HS Fe(III) sites, in agreement with the structural data (vide supra). The drop in moment indicates the presence of intramolecular antiferromagnetic exchange, and since the spin centers are different, a ground state with noncompensated spin would be expected (S_{Tcalc} = 2/2; μ_{SO} = 2.9 μ_B). The value at 2 K is slightly higher than the spin only value, but in good agreement with this model. The variable temperature data were therefore fitted to an isotropic exchange model based on two alternating HS Fe(II), Fe(III) pairs (eq 1), assuming $S_1 = S_3 = 5/2$, $S_2 = S_4 = 4/2$,

dx.doi.org/10.1021/ic201891h | Inorg. Chem. 2011, 50, 12141–12154

and just one exchange integral, J.

$$H_{ex} = -J\{S_1 \cdot S_2 + S_2 \cdot S_3 + S_3 \cdot S_4 + S_1 \cdot S_4\} \quad (1)$$

$$\chi_M = \frac{N\beta^2 g^2}{3k(T-\theta)} \frac{\sum S'(S'+1)(2S'+1)e^{-E(S_r)/kT}}{\sum (2S'+1)e^{-E(S_r)/kT}}(1-\rho) + \frac{N\beta^2 g^2 S(S+1)\rho}{3kT} + \mathrm{TIP} \quad (2)$$

Fitting was accomplished through nonlinear regression using MAGMUN4.1,[46] which derives the spin state/energy profile for the exchange Hamiltonian in question via the van Vleck equation (eq 2; θ = Weiss correction, ρ = paramagnetic impurity fraction, TIP = temperature independent paramagnetism). A good fit was obtained (solid lines in Figure 11) for $g_{av.}$ = 2.26(1), J = −8.7(2), TIP = 200 × 10^{-6} cm^3 mol^{-1}, ρ = 0.018 (10^2R = 1.75; $R = [\Sigma(\chi_{obs} - \chi_{calc})^2/\Sigma\chi_{obs}^2]^{1/2}$). The J value is also reasonable given the range of Fe−O−Fe bridge angles. The good fit indicates that there is no spin crossover of any Fe(II) site in the temperature range studied.

Variable temperature magnetic data for **2** are given in Figure 12, with a moment per mole of 10.4 μ_B at 300 K

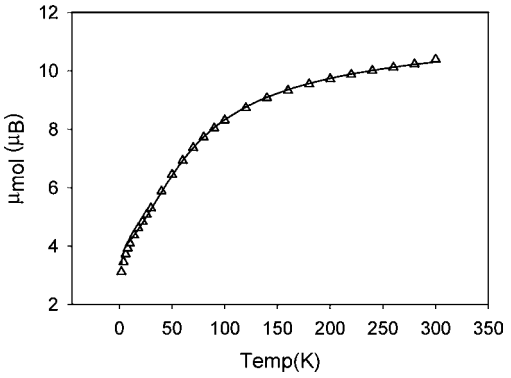

Figure 12. Variable temperature magnetic data for **2**. See text for fitted parameters.

dropping smoothly to 3.1 μ_B at 2 K. Structural data indicate that the iron centers are HS Fe(II). Since only bridging μ-O connections link the apical Fe(II) centers (Fe1, Fe3) to the internal triangular group (Fe2, Fe4, Fe5) with comparable Fe−O−Fe angles, a simple exchange Hamiltonian (eq 3) with one exchange integral was used. A good data fit was obtained using MAGMUN4.1[46] for g = 2.078(8), J = −9.5(1) cm^{-1}, TIP = 900 × 10^{-6} cm^3 mol^{-1}, θ = −1.4 K (10^2R = 0.97).

$$H_{ex} = -J\{S_1 \cdot S_2 + S_1 \cdot S_3 + S_1 \cdot S_4 + S_5 \cdot S_2 + S_5 \cdot S_3 + S_5 \cdot S_4\} \quad (3)$$

The solid line in Figure 12 was calculated with these parameters. The antiferromagnetic exchange clearly occurs via superexchange through the μ-$O_{hydrazone}$ bridging connections, and is consistent with the large Fe−O−Fe angles. There is no evidence for any spin crossover in this case.

Variable temperature magnetic data for **3** are shown in Figure 13. The moment per mole drops from 11.6 μ_B at 300 K to 5.9 μ_B at 2 K, indicating intramolecular antiferromagnetic

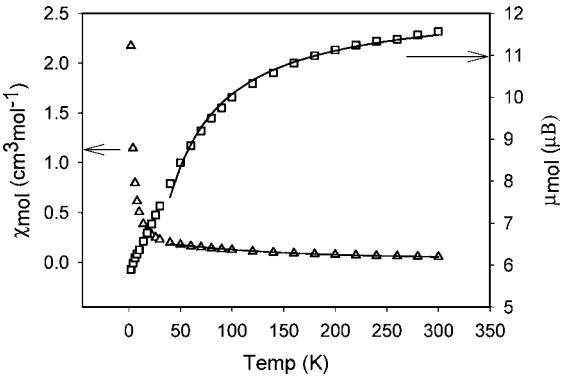

Figure 13. Variable temperature magnetic data for **3**. See text for fitted parameters.

exchange. The rt value is comparable with **1**, but the value at 2 K is substantially higher, suggesting other contributions to the ground state properties. Fitting using eq 1 assuming $S_1 = S_3$ = 5/2, $S_2 = S_4$ = 4/2 was attempted with MAGMUN4.1,[46] but it became apparent that the low temperature region (<40 K) could not be fitted sensibly, with experimental values of the moment being significantly higher than those calculated by the model. Consequently, only data >40 K were fitted to eq 1. A good fit using eq 1 was obtained for $g_{av.}$ = 2.243(9), J = −5.6(1) cm^{-1}, TIP = 580 × 10^{-6} cm^3 mol^{-1}. The solid line in Figure 13 was calculated with these parameters. The nominal ground state according to eq 1 would be 2/2. However, if some low temperature contributions from LS or IS (intermediate spin) Fe(II) sites were operating <40 K, this would have the effect of raising the moment through enhanced spin contributions from the Fe(III) sites. However a formal treatment of this situation did not provide an exact solution in this case, and so the low temperature regime was not modeled.

Variable temperature magnetic data for **3a** are shown in Supporting Information, Figure S2. The moment per mole drops from 13.3 μ_B at 300 K to 5.5 μ_B at 2K, indicating the presence of overall intramolecular antiferromagnetic exchange coupling. However, the two $FeCl_4^-$ anions are magnetically isolated and so would constitute Curie contributions to the total magnetism. The rt moment is close to the spin only value for the sum of two Fe(II) and four Fe(III) sites (13.7 μ_B), in agreement with the structure. The nominal low temperature moment for two Curie sites (S = 4/2) in the antiferromagnetic limit should be 6.91 μ_B. The slightly lower experimental value cannot be associated with any long-range cooperative interactions (vide supra), and so is considered to be associated with single ion properties, for example, zero field splitting. No formal fitting of the magnetic data has been attempted in this case because of the complexity of the overall situation. However, a similar exchange interaction to **3** would be anticipated.

Variable temperature magnetic data for **4** are shown in Figure 14. The moment per mole drops from 9.7 μ_B at 300 K to 2.2 μ_B at 2 K, indicating a spin system dominated by intramolecular antiferromagnetic exchange. The rt value is somewhat smaller than values associated with similar mixed oxidation state grids **1** and **3**, but is consistent with the presence of two HS Fe(II) and HS Fe(III) centers. A successful fitting using eq 1 ($S_1 = S_3$ = 5/2, $S_2 = S_4$ = 4/2) was carried out via MAGMUN4.1[46] giving $g_{av.}$ = 2.00(1), J = −10.3(2) cm^{-1}, TIP = 40 × 10^{-6} cm^3 mol^{-1}, θ = −0.6 K, 10^2R = 1.78. The solid line

dx.doi.org/10.1021/ic201891h | Inorg. Chem. 2011, 50, 12141–12154

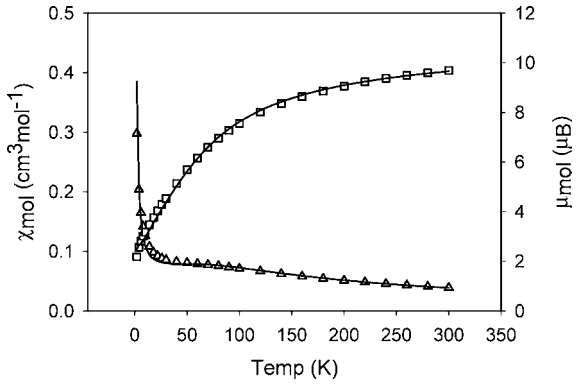

Figure 14. Variable temperature magnetic data for **4**. See text for fitted parameters.

in Figure 14 was plotted using these parameters. Once again the unusual combination of HS Fe(II) and Fe(III) sites, with large Fe−O−Fe bridge angles, leads to substantial antiferromagnetic exchange, and a nonzero ground state ferrimagnetic system. The slight lowering of the moment at 2 K, below the expected value, can be explained by a weak intermolecular antiferromagnetic term (θ = −0.6 K; vide supra).

Variable temperature magnetic data for **5** are shown in Figure 15. The moment per mole of 7.38 μ_B at 300 K is in

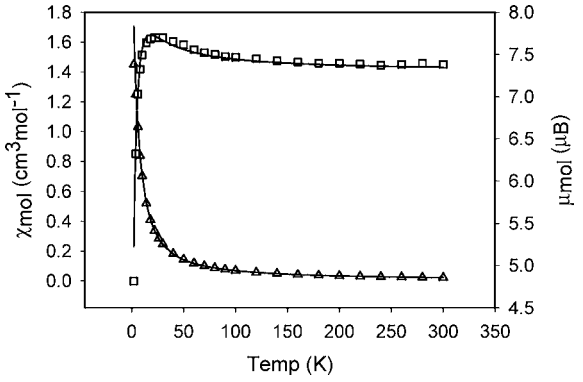

Figure 15. Variable temperature magnetic data for **5**. See text for fitted parameters.

agreement with the presence of two HS Fe(II) centers. It undergoes an unexpected and significant rise as the temperature drops, reaching a maximum of 7.73 μ_B at 18 K, and drops to 4.82 at 2 K. The broad nature of the maximum at this temperature suggests that, although it could be associated with zero field splitting effects, it could also reasonably be assigned to an exchange phenomenon, and suggests the presence of ferromagnetic exchange. The drop below 18 K may however be associated mainly with Fe(II) single ion zero field splitting effects. As an initial attempt at modeling the data, fitting to a simple isotropic exchange equation

$$H_{ex} = -J\{S_1 \cdot S_2\} \quad (4)$$

(eq 4; $S_1 = S_2 = 4/2$) was carried out. This approach gave a surprisingly good fit through MAGMUN4.1[46] for g = 2.106(7), J = 3.1(1) cm^{-1}, TIP = 0 cm^3 mol^{-1}, θ = −4.5 K (10^2R = 1.81). The solid line in Figure 15 was calculated with these parameters. The relatively high θ value might be questioned, particularly since there are no significant longer range contacts in the extended structure, and may be the consequence of ZFS effects. However, the significant positive J value does signal intramolecular ferromagnetic exchange. The structure reveals two important features; the highly asymmetric nature of the dichloro-bridge, and the Fe−O−Fe bridge angle of 96.2°, which is close to the nominal angle of 90° associated with orthogonality effects of the "p" orbital components involved in bridging the Fe(II) centers through the chlorine atoms. The very long Fe1−Cl1′ contacts (2.648(2) Å) would also serve to weaken any antisymmetric overlap of the metal "d" orbitals through these bridges and thus limit any possible contributions from antiferromagnetic effects. A formal inclusion of ZFS terms has not been attempted at this time.

The mononuclear complex **6** has an essentially constant moment of 6.0 μ_B from 300 K down to ∼10 K, followed by a slight drop at lower temperature, clearly indicating HS Fe(III) throughout the temperature range. In contrast the dinuclear complex **7** shows a marked drop in moment from 7.0 μ_B at 300 K to 0.2 μ_B at 2 K. The molar susceptibility shows a very broad maximum at ∼100 K, indicative of a strong antiferromagnetic exchange situation (Figure 16). The two iron

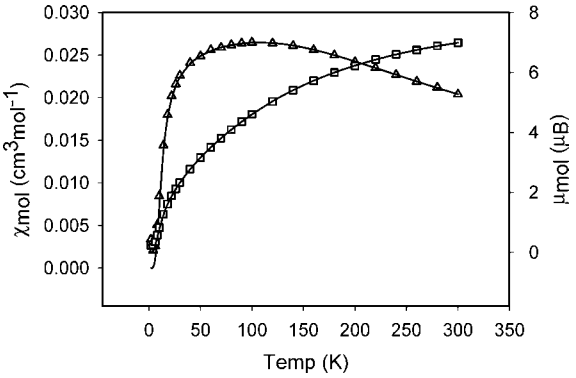

Figure 16. Variable temperature magnetic data for **7**. See text for fitted parameters.

centers are bridged tightly in the dinuclear unit by hydrazone oxygen atoms, with bridge angles of 114.1°. Data fitting through MAGMUN4.1,[46] using an isotropic dinuclear model (eq 4; $S_1 = S_2 = 5/2$) for two S = 5/2 centers, resulted in an excellent fit for g = 2.070(2), J = −26.27(7) cm^{-1}, TIP = 0, θ = 0.5 K (10^2R = 0.40), thus confirming the strong superexchange between the metal ions, and the HS nature of the Fe(III) sites. The solid line in Figure 16 was calculated with these parameters.

Variable temperature magnetic data for **8** show a moment of 6.25 μ_B at 300 K, dropping very slightly down to 50 K (6.0 μ_B), followed by a further small drop at lower temperatures indicative of a mononuclear, Curie-like system. This is typical for a HS Fe(III) species, in agreement with the structure. Variable temperature magnetic data for the dinuclear mixed oxidation state complex **9** are shown in Figure 17, with drop in moment from 7.3 μ_B at 300 K to 1.6 μ_B at 2K, indicating the presence of intramolecular antiferromagnetic exchange. The presence of both a HS Fe(II) and a HS Fe(III) site in such a situation would lead to a nonzero ground state spin situation (S_T = 1/2) in agreement with the experimental data. Data fitting was carried out to eq 3 with S_1 = 5/2 and S_2 = 4/2 to give a very good fit for $g_{av.}$ = 2.136(3), J = −18.7(1) cm^{-1}, TIP = 180 × 10^{-6} cm^3 mol^{-1}, θ = −0.6 K (10^2R = 0.42). Again the strong exchange is consistent with the large Fe−O−Fe bridge angles (vide supra).

dx.doi.org/10.1021/ic201891h | Inorg. Chem. 2011, 50, 12141−12154

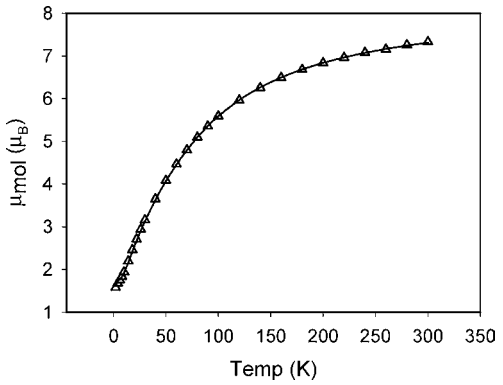

Figure 17. Variable temperature magnetic data for **9**. See text for fitted parameters.

CONCLUSIONS

Ligand directed self-assembly is a powerful synthetic tool and can generate predetermined poly metallic architectures when specifically designed ligands organize metal ions according to their particular coordination algorithms and the matching features of the ligand. The ligand environment generated in such systems is important to the stability of a particular spin state and oxidation state, in terms of the LFSE created, and also to the tendency of a system to exhibit possible spin crossover behavior. Strong field ditopic ligands, for example, L1−L6, involving aromatic heterocycles and also sulfur donors, form [2 × 2] grids which can stabilize LS Fe(II) states, and with the modulation of the crystal field strength can lead to spin crossover behavior. Structural and magnetic data for **2**, **3**, and **5** indicate that both Fe(II) and Fe(III) sites can exist in the same grid, with evidence for possible HS↔LS Fe(II) spin crossover in one case. The tautomeric flexibility of the hydrazone based ligands leads to a variety of assemblies and mononuclear, dinuclear, tetranuclear, and pentanuclear examples have been observed. While oxidation of Fe(II) on complexation by reaction with adventitious oxygen is commonly observed, the ligand itself can have a profound effect on metal redox behavior, and an important observation in the case of these nominally "innocent" ligands is that they can produce reducing conditions, where starting with Fe(III) can lead to the formation of some Fe(II) centers in some cases.

ASSOCIATED CONTENT

Supporting Information

Figure S1; structural representation for **3a**. Figure S2; variable temperature magnetic data for **3a**. Table S1; bond distances and angles for **3a**. This material is available free of charge via the Internet at http://pubs.acs.org.

AUTHOR INFORMATION

Corresponding Author

*Phone: 709-864-8750. Fax: 709-864-3702. E-mail: lk.thompson@mun.ca.

ACKNOWLEDGMENTS

We thank the Natural Sciences and Engineering Research Council of Canada for financial support for this study (L.K.T.).

REFERENCES

(1) Gütlich, P., Goodwin, A., Eds.; *Topics in Current Chemistry*; Springer-Verlag: Berlin, Germany, 2004; Vols. *233*−*235*.
(2) Kahn, O.; Codjovi, E. *Philos. Trans. R. Soc., A* **1996**, *354*, 359−379.
(3) Kahn, O.; Martinez, C. J. *Science* **1998**, *279*, 44−48.
(4) Garcia, Y.; van Koningsbruggen, P. J.; Codjovi, E.; Lapouyade, R.; Kahn, O.; Rabardel, L. *J. Mater. Chem.* **1997**, *7*, 857−858.
(5) Kahn, O.; Codjovi, E.; Garcia, Y.; van Koningsbruggen, P. J.; Lapouyade, R.; Sommier, L. In *Molecule-Based Magnetic Materials*; Turnbull, M.M., Sugimoto, T., Thompson, L.K., Eds.; Symposium Series 644; American Chemical Society: Washington, DC, 1996; pp 298−310.
(6) Gatteschi, D.; Caneschi, A.; Sessoli, R. *Chem. Soc. Rev.* **1996**, 101−109.
(7) Boudalis, A. K.; Donnadieu, B.; Nasopoulos, V.; Clemente-Juan, J. M.; Mari, A.; Sanakis, Y.; Tuschagues, J.-P.; Perlepes, S. P. *Angew. Chem., Int. Ed.* **2004**, *43*, 2266−2270.
(8) Barra, A. L.; Caneschi, A.; Cornia, A.; Fabrizi de Biani, F.; Gatteschi, D.; Sangregorio, C.; Sessoli, R.; Sorace, L. *J. Am. Chem. Soc.* **1999**, *121*, 5302−5310.
(9) Cornia, A.; Fabretti, A. C.; Sessoli, R.; Sorace, L.; Gatteschi, D.; Barra, A. L.; Daiguebonne, C.; Roisnel, T. *Acta Crystallogr.* **2002**, *C58*, 371−373.
(10) Matthews, C. J.; Avery, K.; Xu, Z.; Thompson, L. K.; Zhao, L.; Miller, D. O.; Biradha, K.; Poirier, K.; Zaworotko, M. J.; Wilson, C.; Goeta, A. E.; Howard, J. A. K. *Inorg. Chem.* **1999**, *38*, 5266−5276.
(11) Thompson, L. K.; Matthews, C. J.; Zhao, L.; Xu, Z.; Miller, D. O.; Wilson, C.; Leech, M. A.; Howard, J. A. K.; Heath, S. L.; Whittaker, A. G.; Winpenny, R. E. P. *J. Solid State Chem.* **2001**, *159*, 308−320.
(12) Dawe, L. N.; Thompson, L. K. *Dalton Trans.* **2008**, 3610−3618.
(13) Dawe, L. N.; Abedin, T. S. M.; Thompson, L. K. *Dalton Trans.* **2008**, 1661−1675.
(14) Dawe, L. N.; Abedin, T. S. M.; Kelly, T. L.; Thompson, L. K.; Miller, D. O.; Zhao, L.; Wilson, C.; Leech, M. A.; Howard, J. A. K. *J. Mater. Chem.* **2006**, *16*, 2645−2659.
(15) Milway, V. A.; Abedin, S. M. T.; Niel, V.; Kelly, T. L.; Dawe, L. N.; Dey, S. K.; Thompson, D. W.; Miller, D. O.; Alam, S. M.; Müller, P.; Thompson, L. K. *Dalton Trans* **2006**, 2835−2851.
(16) Dawe, L. N.; Shuvaev, K. V.; Thompson, L. K. *Inorg. Chem.* **2009**, *48*, 3323−3341.
(17) Thompson, L. K.; Zhao, L.; Xu, Z.; Miller, D. O.; Reiff, W. M. *Inorg. Chem.* **2003**, *42*, 128−139.
(18) Thompson, L. K.; Waldmann, O.; Xu, Z. *Coord. Chem. Rev.* **2005**, *249*, 2677−2690.
(19) Parsons, S. R.; Thompson, L. K.; Dey, S. K.; Wilson, C.; Howard, J. A. K. *Inorg. Chem.* **2006**, *45*, 8832−8834.
(20) Dawe, L. N.; Shuvaev, K. V.; Thompson, L. K. *Chem. Soc. Rev.* **2009**, *38*, 2334−2359.
(21) Xu, Z.; Thompson, L. K.; Miller, D. O.; Clase, H. J.; Howard, J. A. K.; Goeta, A. E. *Inorg. Chem.* **1998**, *37*, 3620−3627.
(22) Niel, V.; Milway, V. A.; Dawe, L. N.; Grove, H.; Tandon, S. S.; Abedin, T. S. M.; Kelly, L. K.; Spencer, E. C.; Howard, J. A. K.; Collins, J. L.; Miller, D. O.; Thompson, L. K. *Inorg. Chem.* **2008**, *47*, 176−189.
(23) Breuning, E.; Ruben, M.; Lehn, J.-M.; Renz, F.; Garcia, Y.; Ksenofontov, V.; Gütlich, P.; Wegelius, E.; Rissanen, K. *Angew, Chem., Int. Ed.* **2000**, *39*, 2504−2507.
(24) Ruben, M.; Breuning, E.; Lehn, J.-M.; Ksenofontov, V.; Renz, F.; Gütlich, P.; Vaughan, G. B. M. *Chem.—Eur. J.* **2003**, *9*, 4422−4429.
(25) Gang, H.; Dong, G.; Ding, C.-Y.; Hong, M.; Meng, Q.-J. *New. J. Chem.* **2002**, *26*, 1371−1377.
(26) Zhao, Y.; Guo, D.; Liu, Y.; He, C.; Duan, C. *Chem. Commun.* **2008**, 5725−5727.
(27) (a) Wu, D.-Y.; Sato, O.; Einaga, Y.; Duan, C.-Y. *Angew. Chem., Int. Ed.* **2009**, *48*, 1475−1478. (b) Shuvaev, K. V.; Dawe, L. N.; Thompson, L. K. *Dalton Trans.* **2010**, *39*, 4768−4776.
(28) (a) Anwar, M. U.; Dawe, L. N.; Thompson, L. K. *Dalton Trans.* **2011**, *40*, 8079−8082. (b) Anwar, M. U.; Thompson, L. K.; Dawe, L. N. *Dalton Trans.* **2011**, *40*, 1437−1440.
(29) *SHELX97*; Sheldrick, G. M. *Acta Crystallogr.* **2008**, *A64*, 112−122.

(30) *SIR92*; Altomare, A.; Cascarano, G.; Giacovazzo, C.; Guagliardi, A.; Burla, M.; Polidori, G.; Camalli, M. *J. Appl. Crystallogr.* **1994**, *27*, 435.
(31) Beurskens, P. T.; Admiraal, G.; Beurskens, G.; Bosman, W. P.; de Gelder, R.; Israel, R.; Smits, J. M. M. *DIRDIF99*; The DIRDIF-99 program system, Technical Report of the Crystallography Laboratory; University of Nijmegen: Nijmegen, The Netherlands, 1999.
(32) Cromer, D. T.; Waber, J. T. *International Tables for X-ray Crystallography*; The Kynoch Press: Birmingham, England, 1974; Vol. *IV*, Table 2.2 A.
(33) Ibers, J. A.; Hamilton, W. C. *Acta Crystallogr.* **1964**, *17*, 781.
(34) Creagh, D. C.; McAuley, W. J. *International Tables for Crystallography*; Wilson, A.J.C., Ed.; Kluwer Academic Publishers: Boston, MA, 1992; Vol *C*, Table 4.2.6.8, pp 219−222.
(35) Creagh, D. C.; Hubbell, J. H. *International Tables for Crystallography*; Wilson, A.J.C., Ed.; Kluwer Academic Publishers: Boston, MA, 1992; Vol *C*, Table 4.2.4.3, pp 200−206.
(36) *CrystalStructure 3.7.0*, Crystal Structure Analysis Package; Rigaku and Rigaku/MSC: The Woodlands, TX , 2000−2005.
(37) Watkin, D. J.; Prout, C. K.; Carruthers, J. R.; Betteridge, P. W. *CRYSTALS*, Issue 10; Chemical Crystallography Laboratory: Oxford, U.K., 1996.
(38) Spek, A. L. *J. Appl. Crystallogr.* **2003**, *36*, 7−13.
(39) Hooft, R.; Straver, L. H.; Spek, A. L. *J. Appl. Crystallogr.* **2008**, *41*, 96−103.
(40) (a) *CrystalClear*; Rigaku Corporation: The Woodlands, TX , 1999. (b) *CrystalClear Software User's Guide*, Molecular Structure Corporation, (c) 2000; Pflugrath, J. W. *Acta Crystallogr.* **1999**, *D55*, 1718−1725.
(41) (a) Palenik, G. J. *Inorg. Chem.* **1997**, *36*, 122. (b) O'Keeffe, M.; Brese, N. E. *J. Am. Chem. Soc.* **1991**, *113*, 3226.
(42) Matthews, C. J.; Xu, Z.; Mandal, S. K.; Thompson, L. K.; Biradha, K.; Poirier, K.; Zaworotko, M. J. *Chem. Commun.* **1999**, 347−348.
(43) Matthews, C. J.; Thompson, L. K.; Parsons, S. R.; Xu, Z.; Miller, D. O.; Heath, S. L. *Inorg. Chem.* **2001**, *40*, 4448−4454.
(44) Davies, S. C.; Hughes, D. L.; Leigh, J.; Sanders, J. R.; de Sousa, J. S. *J. Chem. Soc., Dalton Trans.* **1997**, 1981.
(45) Thallaj, N. K.; Machkour, A.; Manodn, D.; Welter, R. *New. J. Chem.* **2005**, *29*, 1555.
(46) MAGMUN4.1/OW01.exe is available from the authors (http://www.ucs.mun.ca/ ~lthomp/magmun). It was developed by Dr. Zhiqiang Xu, and OW01.exe by Dr. O. Waldmann. Source codes are not distributed. The origin of the programs should be quoted.

NOTE ADDED AFTER ASAP PUBLICATION

This paper was published on the Web on October 26, 2011, with the Distances and Angles not represented correctly for Tables 2−10. The corrected version was reposted on October 31, 2011.